


ARTICLE

Mechanical properties of polyvinylpyrrolidone/polyvinyl alcohol-based solid electrolytes

Kingsley Orisekeh^{1,2} | Vitalis Anye¹ | Oluwaseun Oyewole³ |
 Ridwan Ahmed³ | David Orisekeh⁴ | Omolara Oyelade⁵ |
 Sharafadeen Adeniji⁵ | Sadiq Umar² | Abdulhakeem Bello^{1,5} |
 Winston Soboyejo^{1,3} 

¹Department of Materials Science and Engineering, African University of Science and Technology, Abuja, Nigeria

²National Space Research and Development Agency (NASRDA), Obasanjo Space Centre, Abuja, Nigeria

³Department of Mechanical Engineering, Worcester Polytechnic Institute, Worcester, Massachusetts, USA

⁴Department of Mechanical Engineering, Miami University, Oxford, Ohio, USA

⁵Department of Theoretical and Applied Physics, African University of Science and Technology (AUST), Abuja, Nigeria

Correspondence

Abdulhakeem Bello and Winston Soboyejo, Department of Materials Science and Engineering, African University of Science and Technology, Abuja, Airport Road, Federal Capital Territory, Nigeria.
 Email: abello@aust.edu.ng and wsoboyejo@wpi.edu

Funding information

Pan African Materials Institute, Grant/Award Number: 2015 5415-NG

Abstract

The demand for flexible, lightweight, and long-lasting energy devices has stimulated interest in solid polymer blends. The conventional lithium-ion batteries use liquid electrolytes that are chemically unstable due to the presence of carbonates, which are highly volatile and flammable, creating a significant safety risk. Therefore, the need for the development of solid-state electrolytes that are safe, environmentally friendly, with robust mechanical properties. In this work, the solid polymer blend is explored using a mixture of a polymer matrix of polyvinylpyrrolidone/polyvinyl alcohol and lithium perchlorate salt. The produced films are characterized using a scanning electron microscopy, X-ray diffraction, and Fourier transform infrared. The mechanical properties of the flexible films are also measured using nanoindentation techniques, statistical deconvolution mapping, tensile tests, and fracture toughness measurements. (Young's modulus of 6.87 GPa, hardness of 1.3 GPa, tensile strength of 4.3 MPa, and fracture toughness of 0.81 MPa.m^{0.5}) The implications of the results are then discussed for potential applications of robust solid polymer blends-based electrolytes.

KEYWORDS

composites, films, mechanical properties, morphology, structure–property relationships

1 | INTRODUCTION

The worldwide trend in the continuous demand and efficient use of renewable technologies especially in portable electronic devices, the rapid development and expansion of the electric vehicle market in the last decade signals the importance of energy storage technologies, particularly lithium-ion batteries (LiBs). The conventional LiBs use liquid electrolytes and plays a major role in the market. However, there are significant fire and explosion

risks that are associated with the chemical instability of liquid electrolytes, for example, due to the presence of carbonates that are highly volatile and flammable.^{1,2}

Solid electrolytes (SEs) offer promising and viable alternatives that reduce the safety risks associated with the use of liquid electrolytes. Among all SEs, polymer-based SEs are preferred because of their low flammability, good flexibility, excellent thermal stability, and high safety.

Although prior research efforts^{3,4} have shown that solid polymer-based electrolytes enhance electrochemical

performance, the relatively low-ionic conductivities and poor mechanical properties of SEs still remain a major challenge that must be overcome. In order to address these challenges and enhance the performance of SEs, several composites (reinforced with particles) have been explored as electrolytes in polymer-based blends.^{5,6} Nevertheless, there have been only limited studies of the mechanical properties of polymer-based solid electrolytes. Hence, in this work, we will focus on the mechanical properties of a PVA/PVP/LiClO₄ solid polymer blend, with the aim of addressing this knowledge gap. It is important to study the mechanical properties of solid-state electrolyte (SSE) to give an understanding of the behavior of the blends to applied load.

The quest for novel solid polymer electrolytes (SPEs) has evolved into the use of polymers such as polyvinyl alcohol (PVA), polyvinylpyrrolidone (PVP), polyethylene glycol (PEG), polyacrylonitrile (PAN), polyethylene oxide (PEO), and polyvinylidene fluoride (PVdF) in energy storage.⁷ Sundaramahalingam et al.⁷ noted that “most of the industries uses poly (vinyl alcohol) (PVA) as an effective polymer matrix to achieve the desired properties,” while Abdelrazek et al.⁸ doped PVA with phosphoric acid and applied it as electrolyte in solid-state photocells and solid-state electrochromic displays.

In this work, we explore the development of SE using a mixture of host polymers of PVP, PVA and lithium perchlorate (LiClO₄) integrated into flexible and lightweight-transparent films. The mechanical properties of the films are studied using nanoindentation techniques and statistical deconvolution mapping, tensile tests, and fracture toughness measurements.

Yoon et al.⁹ carried out mechanical tests to measure the fracture properties of the solid electrolyte interphase (SEI) on lithium metal anodes in LiBs. These are made up of electrolyte additives, such as ethylene carbonate (EC) and fluoroethylene carbonate (FEC). Atomic force microscopy (AFM) and membrane-bulge configurations were then combined to determine the stress-strain behavior of SEI, as well as the onset of inelastic response and the initiation of fracture in the two different electrolytes (1.2 M LiPF₆ in EC and 1.2 M LiPF₆ in EC/FEC [8:2]). This was used to study the effects of the FEC additive). The mechanical properties of SSE have also been shown to have a major effect on the performance of energy storage systems.^{9–15}

Yan et al.¹⁶ have used depth-controlled indentation mapping tests to study the mechanical properties of the solid electrolyte material (Li_{1.3}Al_{0.3}Ti_{1.7}[PO₄]₃) {LATP} along different loading axes. The nanoindentation surface profiles were studied after the indentation of the ceramic

electrolyte (with a rhombohedral crystal structure). The Young's moduli and hardness values (calculated using the Vlassak-Nix model¹⁶) were compared with experimentally determined Young's moduli and hardness values. The experimental results were in good agreement with the predictions from the model. However, there were slight differences between the extreme value of 118–177 GPa (obtained for the model) and the experimental results of 114–160 GPa.¹⁶

Fincher et al.¹⁷ have also studied the mechanical properties of metallic lithium using nanoindentation measurements and bulk tensile testing. They reported that bulk Li has a yield strength between 0.57 and 1.26 MPa, for strain rates between $5 \times 10^{-4} \text{ s}^{-1}$ and $5 \times 10^{-1} \text{ s}^{-1}$. They also reported a decrease in the hardness from 43 to 7.5 MPa, as the indentation depth increases from 250 nm to 10 μm , in the case of indentation tests with loading $P/P = 0.05 \text{ s}^{-1}$.

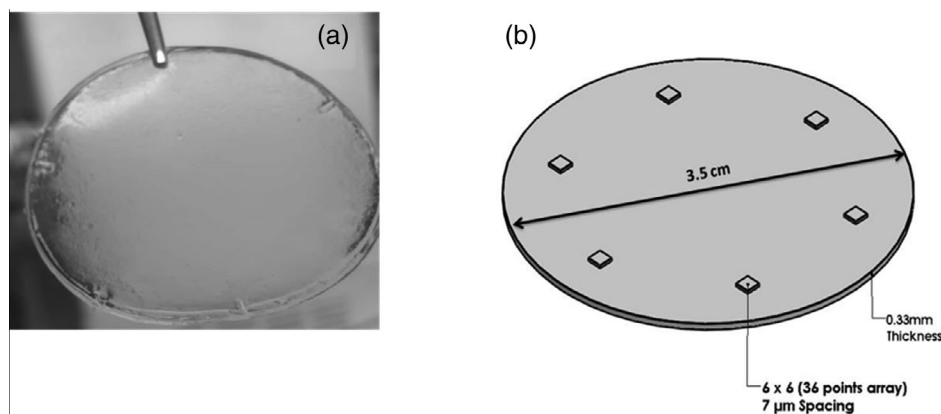
However, to the best of our knowledge, there has been no prior work on the mechanical properties of PVA/PVP/LiClO₄ polymer-based solid electrolytes that are being considered for potential applications in charge storage. Thus, the major objective of this work is to study the mechanical properties of PVA/PVP/LiClO₄ polymer-based SEs. This will be done using a combination of tensile, nanoindentation and fracture toughness measurements to determine the strength, Young's moduli, hardness, and fracture toughness values of solid blends of PVP/PVA and Lithium perchlorate salt. The Oliver and Pharr method^{18,19} will be used to study the spatial variations in the local mechanical properties. These will then be analyzed using statistical deconvolution techniques that will be used to extract the mechanical properties of the materials in the composite blends.^{13,20–23} Finally, the fracture mechanisms and the crack/microstructure interactions associated with the fracture of the blends will be elucidated before discussing the implications of the current work for the design of mechanically robust PVA/PVP/LiClO₄ polymer-based solid electrolyte.

2 | MATERIALS AND METHODS

2.1 | Materials

The chemicals and reagents were of analytical grade and used as received without any further purification. The PVA with Mw 89,000–98,000 g/mol (99+ % hydrolyzed), PVP with Mw 55,000 g/mol, and Lithium perchlorate (LiClO₄) salt were all purchased from Sigma-Aldrich Company, St. Louis, MO. Distilled water was used for the preparation of the samples.

FIGURE 1 (a) Flexible transparent film and (b) 3-D design of flexible film with solid works software



2.2 | Preparation of the solid polymer blend

PVA, PVP, and lithium perchlorate were prepared according to⁷ with some modifications. 0.5 g of PVA and 0.5 g of PVP were dissolved in 25 g of distilled water separately which constitute 2 wt% of each solution. Afterwards, x grams of lithium perchlorate ($x = 0.1, 0.2, 0.3, 0.4$ and 0.5) dissolved in 10 g of distilled water which are made up of various compositions of 1, 2, 3, 4, and 5 wt% respectively. First, the PVA precursor was measured in a beaker and distilled water was added appropriately. Distilled water was used as a preferred choice of solvent for the polymers dissolution to avoid introducing counter ion effect in using other solvents like dimethyl sulfoxide (DMSO) and dimethylformamide (DMF).

The mixture was heated at 90°C with stirring at 350 rpm for 1 h and continued stirring without heat at 350 rpm for 4 h to obtain a homogeneous transparent solution. Similarly, PVP and lithium acetate solutions were prepared separately following the same procedure for the PVA without heating. Each of the solutions prepared were mixed and stirred for 24 h to obtain a homogeneous solution. Finally, the solution was then poured into polypropylene dish and dried at ambient. The flexible uniform and transparent films obtained was kept in a desiccator after drying for further characterization. Figure 1a shows a picture of one of the obtained transparent and uniform films while Figure 1b shows the 3-D design with Solid works software (LULZBOT TAZ 6, Fargo, ND).

2.3 | Tensile tests

Tensile tests were carried out on both the bare PVA–PVP and doped films using Servohydraulic Instron machine (Instron 8872, Instron, Norwood, MA) which was instrumented with a 10 N load cell. The tensile tests were

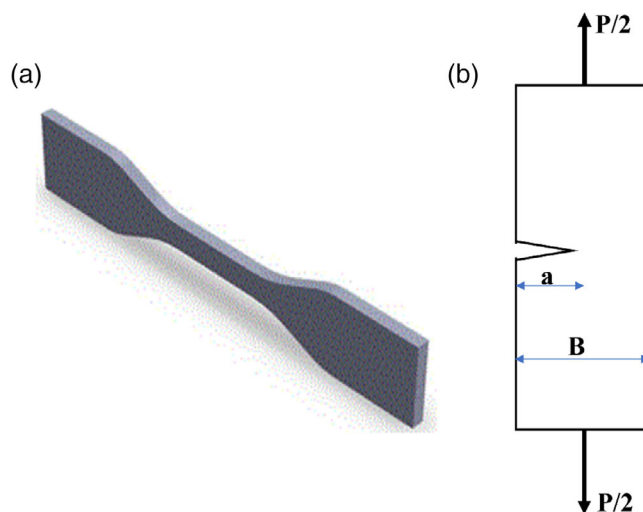


FIGURE 2 (a) Dog-bone specimen (b) schematics diagram of single edge notched specimen under tension [Color figure can be viewed at wileyonlinelibrary.com]

carried out on dog-bone specimens (Figure 2a) that were deformed at a crosshead speed that corresponds to a strain rate of $4 \times 10^{-2} \text{ s}^{-1}$.

2.4 | Fracture tests

To estimate the fracture toughness of the flexible polymer blend, we carried out fracture tests on a single edge notched specimen under tension using Instron testing machine (Instron 68SC-1, Norwood, MA). Figure 2b presents the schematics of the single edge notched specimen used for the measurements. The crosshead of the instrument was operated at a speed of 2 mm/min to strain the samples using a very sensitive calibrated 10 Newton load cell. The test was performed for the polymer blends with different concentrations of the lithium perchlorate (LiClO_4) salt.

$$K_{Ic} = \frac{P}{B\sqrt{w}} \left\{ \frac{\sqrt{2 \tan \left[\frac{\pi a}{2w} \right]}}{\cos \left[\frac{\pi a}{2w} \right]} \left[0.752 + 2.02 \left[\frac{a}{w} \right] \right. \right. \quad (1)$$

$$\left. \left. + 0.37 \left[1 - \sin \left[\frac{\pi a}{2w} \right] \right]^3 \right] \right\},$$

where K_{Ic} is the fracture toughness, P is the force, a is the notch length, w is the width of the material while B is the thickness of the material.

2.5 | Nanoindentation measurements

The flexible uniform and transparent films were mounted on steel stage for indentation test. The indentation experiments were used to measure the Young's moduli and hardness values of the SSE (PVA/PVP/LiClO₄). The resulting films had an average thickness of ~0.33 mm, measured using a micrometer screw gauge. The indentation measurements were carried out on all the prepared films while maintaining a relative humidity of less than 5% to prevent the film from absorbing moisture within the environment using the TI950 Triboindenter (Hysitron Inc., Minneapolis, MN), coupled to a Dimension 3100 scanning probe microscope (Veeco Instruments Inc., Woodbury, NY), (A Berkovich indenter tip, a three-sided pyramidal-type tip, with an included angle of 142.3°) was used for indentation testing. The choice of the Berkovich indenter was because of its large included angle which tends to increase the contact area with the samples. The indentation loading profile included the following three steps: loading to a peak load in 10 s; holding at the peak load for 5 s, and returning to zero load in 10 s. A peak load ranging from 500 μN to 1000 μN was applied. Grid indentation with multi-points using a 6 × 6 (36 points array) matrix mapping was carried out to determine the average elastic modulus and average hardness of the sample. The same load function was set for each experiment in the grid. To minimize the possible interactions between adjacent indents, all the indents were separated by at least 7 μm. A contact-based scanning probe method was used to capture the images of the surfaces before and after the indentation.

The indentation depths were generally much greater than the surface roughness levels. Commonly, for metallic materials, indentation depths should be at least 20 times greater than the average surface roughness to minimize the possible effects of rough surfaces.²⁴ Also,

the, indentation depths should be less than 10% of the film thickness to minimize substrate effects,¹⁹ especially for those films harder than the substrate.

In this study, a range of peak loads was selected, which generated a range of contact depths during the indentation experiments, to study the possible effects of indentation depth. Finally, the peak loads were maintained for sufficient durations to minimize the possible effects of viscoelasticity on the measured elastic moduli.

In addition to determining the elastic modulus and hardness, loads above the peak values were applied for possible inducement of cracks within the layers to study the fracture toughness of the samples. The images of the samples were viewed using a scanning probe microscope (SPM) attached to the Triboindenter. Furthermore, statistical deconvolution mapping was carried out to further determine the mechanical properties using its toolbox in Matlab software (MATHWORKS Inc. Natick, MA).

2.6 | Materials characterization

The surface morphology of the samples was characterized using a scanning electron microscope (SEM, ZEISS EVO LS10 MA). The crystallinity of the samples was carried out using a Malvern PANalytical X-ray diffractometer (XRD) (Malvern PANalytical, Westborough, MA), equipped with a Cu K α radiation source and a Beta Nickel filter that was operated at 40 kV and 40 mA in the 2 θ range (2 θ = 10–90°). Fourier transform infrared (FTIR) measurements were used to obtain the transmittance spectra of the films. These were obtained using a QATR-S single reflection integration type ATR accessory with a diamond crystal (QATR-S, Shimadzu, USA) with a wave number range of 500–4000 cm⁻¹.

3 | RESULTS AND DISCUSSION

3.1 | Microstructure

The surface morphologies of the uniform and flexible transparent films are presented in Figure 3a–f. Figure 3a shows a uniform rough surface for the blend of PVA/PVP. In Figure 3b–f, the uniform roughness of the film surfaces increases due the dissolution of salt (LiClO₄) in the blend polymer film. As the amount of salt is increases, some crystallites are also observed in blend polymers. This is clear from the XRD results, which shows that the PVA/PVP is amorphous in nature. The differences in the surface morphologies are attributed to the oxidation and interactions of the functional groups

FIGURE 3 SEM micrographs (a) PVA + PVP (b) PVA + PVP + 1 wt% LiClO₄ (c) PVA + PVP + 2 wt% LiClO₄ (d) PVA + PVP + 3 wt% LiClO₄ (e) PVA + PVP + 4 wt% LiClO₄ (f) PVA + PVP + 5 wt% LiClO₄. LiClO₄, lithium perchlorate; PVA, polyvinyl alcohol; PVP, polyvinylpyrrolidone; SEM, scanning electron microscope

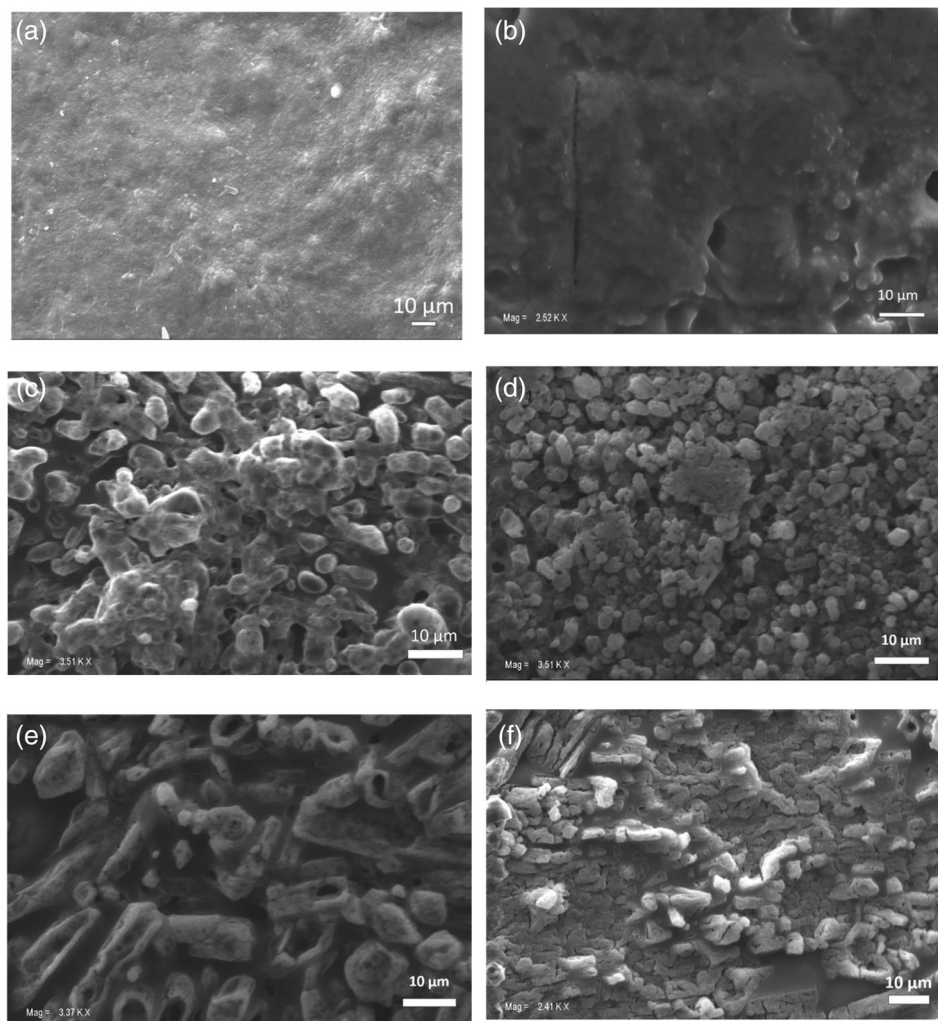
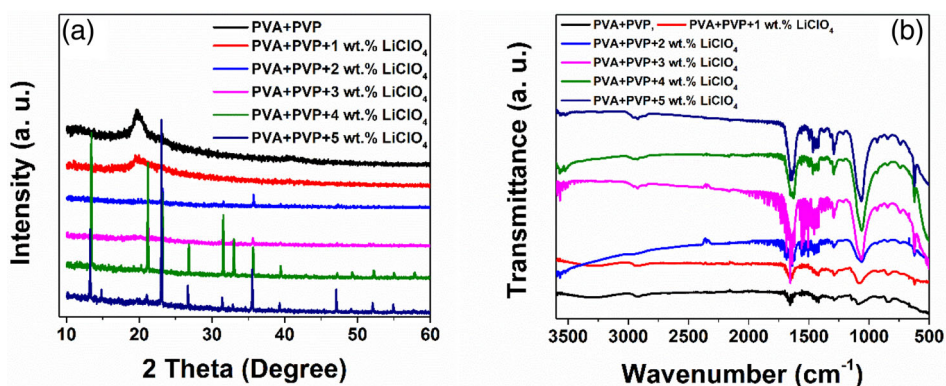


FIGURE 4 (a) XRD patterns of 2 wt% PVA: 2 wt% PVP with blends of various concentrations of lithium perchlorate. (b) FTIR spectra of 2 wt% PVA: 2 wt% PVP with blends of various concentrations of lithium perchlorate. FTIR, Fourier transform infrared; PVA, polyvinyl alcohol; PVP, polyvinylpyrrolidone; XRD, X-ray diffractometer [Color figure can be viewed at wileyonlinelibrary.com]



that are present in the polymer blend (presence of hydroxyl group of PVA and carbonyl group of PVP) with different salt contents. The roughness and crystallinity can also be explained by the distribution of the salt in the blended polymer matrix.

X-ray diffraction (XRD) patterns of the flexible transparent films are presented in Figure 4a. PVA has been

reported to be semi-crystalline in nature with peaks appearing at 20° and 40°.^{7,25} From Figure 4, the polymer blend of PVA/PVP has peaks at $2\theta = 19.6^\circ$ and 40.2° . These are associated with the long chain carbon backbone and amorphous nature of the PVA in the polymer blends with PVP. However, the amorphous nature of the polymer blend changes, as the concentration of lithium

perchlorate increased in the matrices, this is as a result of the complex bond of $\text{Li}^+ \dots \text{C}=\text{O}$ (short range of LiClO_4 in the matrix of PVA/PVP blend).^{26,27}

Hence, increasing the concentration of the LiClO_4 increases the crystallinity of the compositions. It was also observed that the interactions of the functional groups present in PVA/PVP and the dopant ions from LiClO_4 (Li^+ and ClO_4^-) leads to the displacement of the ions from their lattice sites which is responsible for the shifts in peaks and crystallinity of the composition.²⁸

The above interactions, as well as the bond formations of the polymer blends and the compositions of the matrices with the LiClO_4 , were investigated with the FTIR spectroscopy. The IR spectra of the films with different concentrations of the LiClO_4 are presented in Figure 5b.

The band observed at $\sim 1564 \text{ cm}^{-1}$ originate from PVP and is attributed to the characteristics vibration of pyridine ring ($\text{C}=\text{N}$) while the transmission band at 844 cm^{-1} is associated with the out-of-plane rings of $\text{C}=\text{H}$ bending. The pure PVA has its transmission band at 3340 cm^{-1} due to the $\text{O}=\text{H}$ stretching vibration of hydroxyl group which is consistent with literature.^{7,26,29} The respective IR bands of the polymer blend at 3340, 2932, 1646, 1419, 1020, and 928 cm^{-1} are due to the $\text{O}-\text{H}$ stretching, $(\text{C}-\text{H})_n$ asymmetric stretching, $\text{C}=\text{O}$ stretching, CH_2 bending, $\text{C}-\text{O}$ stretching, and $\text{C}-\text{O}$ symmetric stretching, respectively.^{7,8} The shift of $\text{C}=\text{O}$ bond signal is also due to the hydrogen bond between $\text{C}=\text{O}$ and OH groups.

This is in agreement with the XRD results (Figure 4a). The shape and intensity of the bands also

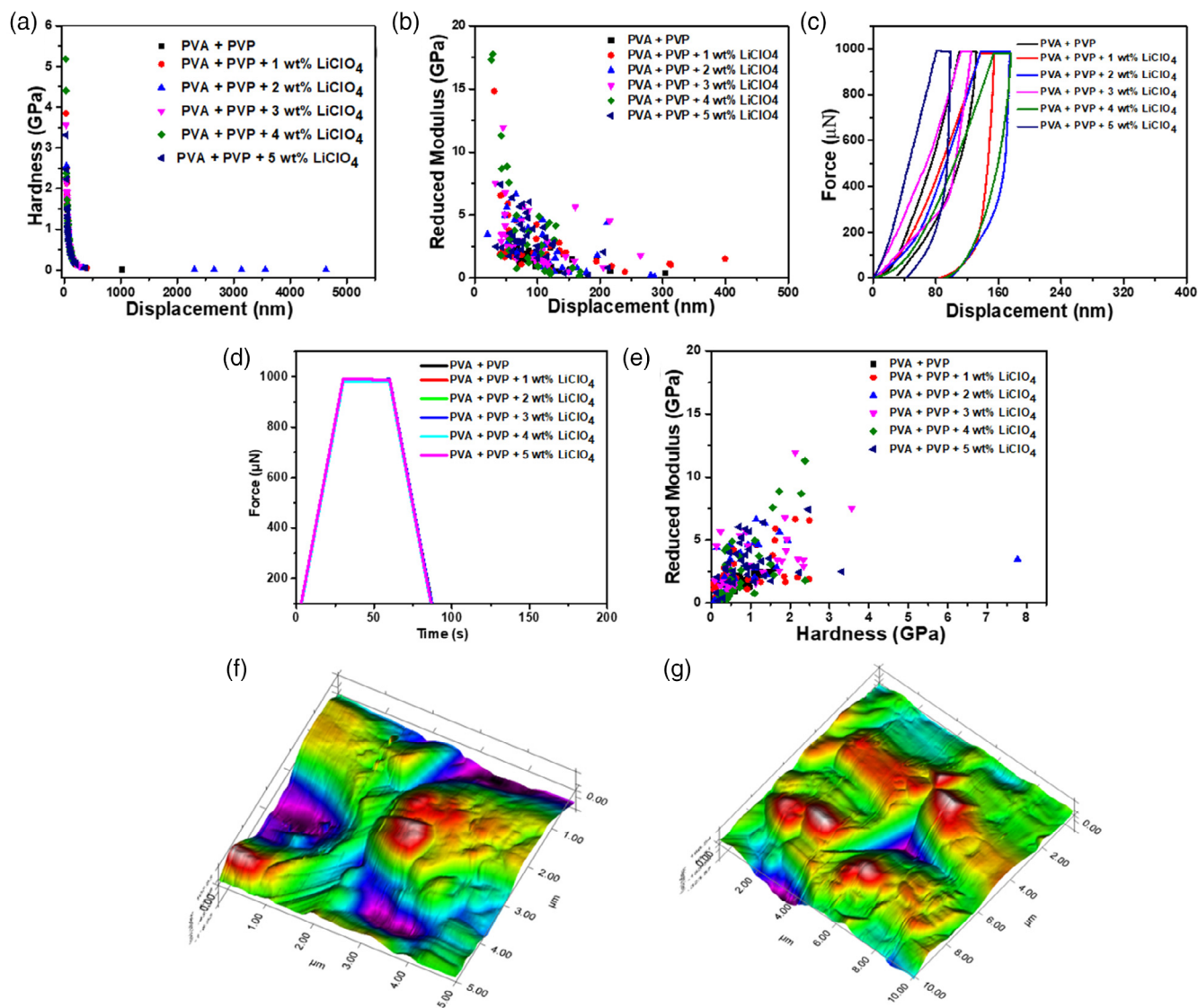


FIGURE 5 Indentation plots (a) hardness versus displacement (b) elastic modulus versus displacement (c) force versus displacement (d) force versus time (e) elastic modulus versus hardness (f) 3-D image of polymer blend before indentation (g) 3-D image of polymer blend after indentation [Color figure can be viewed at wileyonlinelibrary.com]

increases as the concentration of LiClO_4 increases, this is responsible for the transition from the semi-crystalline of the polymer blend to the crystalline nature of the electrolyte. At $\sim 1647\text{ cm}^{-1}$, the presence of the vibrational band corresponds to the C—O symmetric bending of PVA and PVP.^{7,14} Peaks from 1640 to 1649 cm^{-1} regions are attributed to shift in stretching modes of the carbonyl bonds, as a result of the pyrrolidone rings. In summary, it can be inferred that the shifts and variations in the intensities of the FTIR spectra (of the electrolyte compositions) describe the complexities of the salt and polymer blends.^{7,8}

3.2 | Indentation measurements and fracture toughness

A summary of the Young's moduli (E), hardness (H) values and fracture toughness values obtained from this study is presented in Table 1, which also includes the ratio E/H. It is interesting to note here that the concentration of the salt (LiClO_4) in the blends of the polymer matrix (PVA/PVP) increased until an optimal value was reached. It then decreased with increasing salt concentration. This can be attributed to the formation of stronger bonds between the polymer matrix and the salt as the salt concentration increases. However, beyond the optimal value of salt concentration, the drop in the values of E and H indicates that the composite material becomes brittle.

On the other hand, as shown in Figure 5a, the contact depth decreases as the concentration of the salt (LiClO_4) in the blend of the polymer matrix (PVA/PVP) increases until an optimal value and then increases. The reason for decrease in contact depth implies that the material has a high strength and high resistance to deformation, a characteristic needed to suppress any dendrite growth of Li metals and boost large-scale device production.^{30–32}

Figure 5a shows the plot of hardness (GPa) as a function of the displacement (nm). It is observed that the hardness decreased as the displacement increased. This is due to decrease in contact depth and roughness of the material. Similarly, in Figure 5b, the plot of reduced modulus (GPa) against displacement (nm) shows that the modulus decreases as the displacement increases. Figure 5c,d presents a plot of the Force (μN) as a function of the displacement (nm). These show the loading, hold and unloading times of each concentration of the film, all emanating from the origin. Figure 5e presents plots of reduced modulus (GPa) against Hardness (GPa). It was observed that both properties increased with increasing concentration of the salt (LiClO_4) in the blends up to an optimal value at PVA/PVP/4 wt% LiClO_4 , beyond which and the properties decreased. Figure 5f,g presents respective 3-D images of the solid electrolyte before and after indentation. A peak load of $5000\text{ }\mu\text{N}$ (as against the initial $1000\text{ }\mu\text{N}$ load used) was applied. However, no visible crack was observed after the application of this load.

To further elucidate the fracture behavior of the flexible polymer blend, the fracture toughness was measured using a single edge notched specimen. Figure 6a presents the force-displacement curves for the control (PVA + PVP) and polymers with different proportions of LiClO_4 . The results show that the blends with incorporation of 1%–2% of LiClO_4 salt have similar ductile behavior as the control specimen with evident of low strength. The force-displacement curves are very close (Figure 6a). However, the strength increased with increasing proportion of the salt from 2% to 4%. The ductility of the polymer blend also decreases with increasing concentration of the salt. At higher concentration (up to 5%), the strength of the flexible polymer blend is reduced (Figure 6a). The decrease in the strength at 5 wt% can be associated with inhomogeneity of the excessive powder in the blend which can create pathways for crack initiation and propagation. It is important to note that a

TABLE 1 Indentation measurements and tensile tests of the PVA/PVP/ LiClO_4 blend at different salt concentration

Sample	Young's modulus (GPa)	Hardness (GPa)	Fracture toughness ($\text{MPa}\cdot\text{m}^{0.5}$)	E/H	Tensile strength (MPa)
PVA/PVP (50/50)	1.72	0.53	0.32	3.25	7.85
PVA/PVP + 1 wt% LiClO_4	2.40	0.57	0.45	4.22	1.44
PVA/PVP + 2 wt% LiClO_4	2.70	0.63	0.5	4.29	1.34
PVA/PVP + 3 wt% LiClO_4	4.11	0.92	0.76	4.47	3.00
PVA/PVP + 4 wt% LiClO_4	6.87	1.3	0.81	5.29	4.30
PVA/PVP + 5 wt% LiClO_4	4.14	0.91	0.78	4.55	1.51

Abbreviations: LiClO_4 , lithium perchlorate; PVA, polyvinyl alcohol; PVP, polyvinylpyrrolidone.

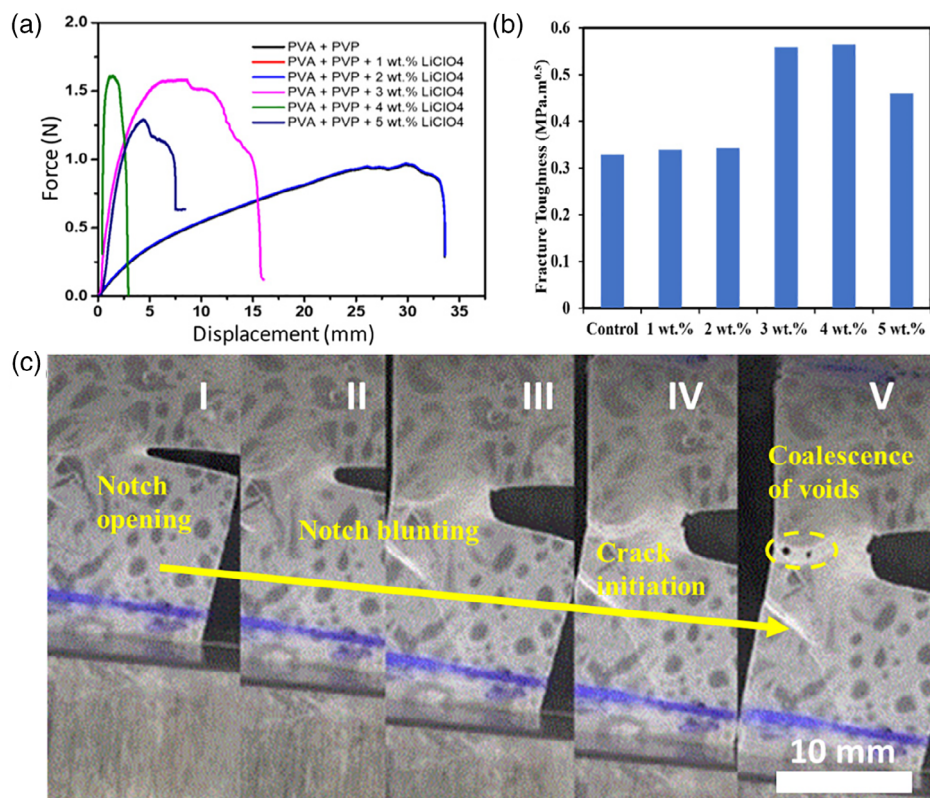


FIGURE 6 (a) Plots of force-displacement curves, (b) fracture toughness values and (c) optical images of failure mechanisms during fracture of the flexible polymer blends [Color figure can be viewed at wileyonlinelibrary.com]

TABLE 2 Summary of the fracture toughness values using single edge notched specimen under tension result

Sample	Toughness (MPa.m ^{0.5})
PVA + PVP	0.3286
PVA + PVP + 1 wt% LiClO ₄	0.3392
PVA + PVP + 2 wt% LiClO ₄	0.3424
PVA + PVP + 3 wt% LiClO ₄	0.5588
PVA + PVP + 4 wt% LiClO ₄	0.5649
PVA + PVP + 5 wt% LiClO ₄	0.4590

Abbreviations: LiClO₄, lithium perchlorate; PVA, polyvinyl alcohol; PVP, polyvinylpyrrolidone.

balance is needed between the strength and ductility of the reinforced LiClO₄ salt—flexible polymer blend for a desired functionality.

The fracture toughness of the polymers was estimated using Equation (1). Figure 6b presents the results of the fracture toughness values for control and LiClO₄ incorporated flexible polymer blends. The results are also summarized in Table 2. The results show that the fracture toughness of the polymer blends increased as the concentration of the salt increases from 0% to 4%. The increase in the toughness is attributed to the formation of stronger bonds between the polymer matrix and the salt. The optimal value of the toughness was recorded for polymer with 4 wt% concentration of

the salt. We observed a drop in fracture toughness value for flexible polymer with 5 wt% concentration.

The trends in the fracture toughness results obtained from the single notched samples are in agreement with the result obtained from the fracture toughness obtained from the nanoindentation technique (Table 1). The optical images of the failure mechanisms of the fractured flexible polymer blends are presented in Figure 6c (I, II, III, IV, and V). As the notch opens, we see evidence of tip blunting before crack initiation. There is also evidence of voids formation that coalesced to form big cracks. The trends in the measured Young's moduli and hardness values also imply that the control of the blend mixtures can be used to engineer the design of robust films with attractive combinations of strength, Young's moduli and fracture toughness.

3.3 | Tensile tests

The tensile test was performed for the polymer blends with different concentrations of the lithium perchlorate (LiClO₄) salt and the results of the tensile strength is presented in Table 1 and Figure 7. From Table 1, the tensile strength for the PVA + PVP blend is higher than what was obtained after the addition of the different concentrations of the LiClO₄ salts; this is due to less impact of elastic deformation and elongation of the polymer chains. It also demonstrates better comparative ductility

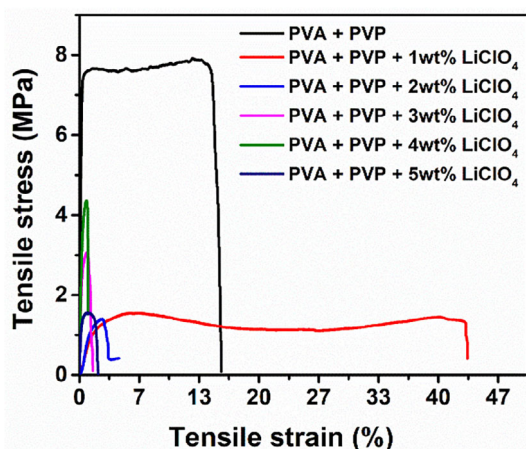


FIGURE 7 Plot of tensile stress (MPa) versus tensile strain (%) [Color figure can be viewed at wileyonlinelibrary.com]

and toughness as seen from the area under the curve in Figure 7 as well as good linear relationship between the stress and strain.

The addition of 1 wt% LiClO_4 salt to the polymers blend results to significant reduction in the tensile strength due to weak intermolecular interaction as well as poor adhesion at the interface of the blends.³³ It was also observed that this increased the ductility of the material due to further elongation of the polymer chains. There was an irregularity of tensile strength behavior at 2 wt% LiClO_4 which could be attributed to the presence of defects as reported by Sallal et al.⁴ The tensile strength value increased with the highest value recorded at the concentration of 4 wt% LiClO_4 and then reduced at the addition of 5 wt% LiClO_4 due to reduction in the crystallinity as seen in the XRD pattern of Figure 4a.

The above trend shows that the complex formed at the addition of 4 wt% LiClO_4 gave an optimal tensile strength of the polymer blends with the salt (which is in agreement with the results of the hardness, Young's modulus and fracture toughness performed with the Nano indentation tests in Table 1). This is due to stronger bonds formed from the interactions of the various functional groups present as seen in the FTIR analysis (Figure 4b). Also, the XRD analysis (Figure 4a) reveals that increasing the particle loading of the polymer blends increases the crystallinity of the resultant composite which further explains the increase in the tensile strength as the salt concentration is increased from 1 to 4 wt%.

3.4 | Deconvolution and mapping using statistical deconvolution

The mapping from the indentation test to determine the tribological properties of the PVA/PVP/ LiClO_4 blend of

the polymer blend are presented in Figure 8a–d. The mapping was implemented using Matlab Software (MATWORKS Inc. Natick, MA) to extract the values of the Young's modulus and hardness values from the multiple grids in the indentation test.

Figure 8a shows the statistical deconvolution mapping of elastic modulus (GPa) in the x and y coordinates (μm) respectively with 6 points of indents along x-axis as well 6 points of indents along y/z axis making a total of 36 points array. The distance between indents (along both axis) was 7 μm . Also, the Young's modulus (in GPa) differentiated with color bars having a mean property value of 11.57 GPa. (± 46.75) as shown in Table 3. Figure 8b presents the statistical mapping of hardness (GPa) in the x and y coordinates (μm), respectively, with the distance between indents in both axis being 7 μm , while the hardness (GPa), differentiated with color bars, had a mean value of 6.01 GPa. (± 3.8) as tabulated in Table 3.

Figure 8c shows the statistical deconvolution mapping of the plots of elastic modulus (GPa) versus hardness (GPa). The elastic modulus has a direct correlation with hardness. This result is in agreement with the nanoindentation calculated result which is attributed to the formation of stronger bonds between the polymer matrix and the salt. The variance in the nanoindentation calculated result and statistical deconvolution result could be as a result of the large size of the 36 points array.

Figure 8d The plot of probability density function (PDF) and cumulative density function (CDF) against hardness (GPa) showing the changes in phase in the histogram tabulated in Table 4. The results suggest the improvement in the mechanical properties from phase 1 to phase 2.

4 | SUMMARY AND CONCLUDING REMARKS

This article presents the mechanical properties of PVA/PVP/ LiClO_4 blends that are being explored as solid electrolytes in energy storage systems. Optimal reduced Young's modulus and hardness values (6.87 GPa and 1.30 GPa, respectively) and the fracture toughness estimates of $0.81 \text{ MPa}\cdot\text{m}^{0.5}$ were obtained. The results shows that the moduli (E) and hardness (H) values of the materials, as well as the ratio, E/H, and the fracture toughness, increased as the concentration of the salt (LiClO_4), in the blend of the polymer matrix increases. These increases continue until the minimum contact depth is reached. The contact depth then increased with increasing PVA/PVP proportions. Also, the combination of

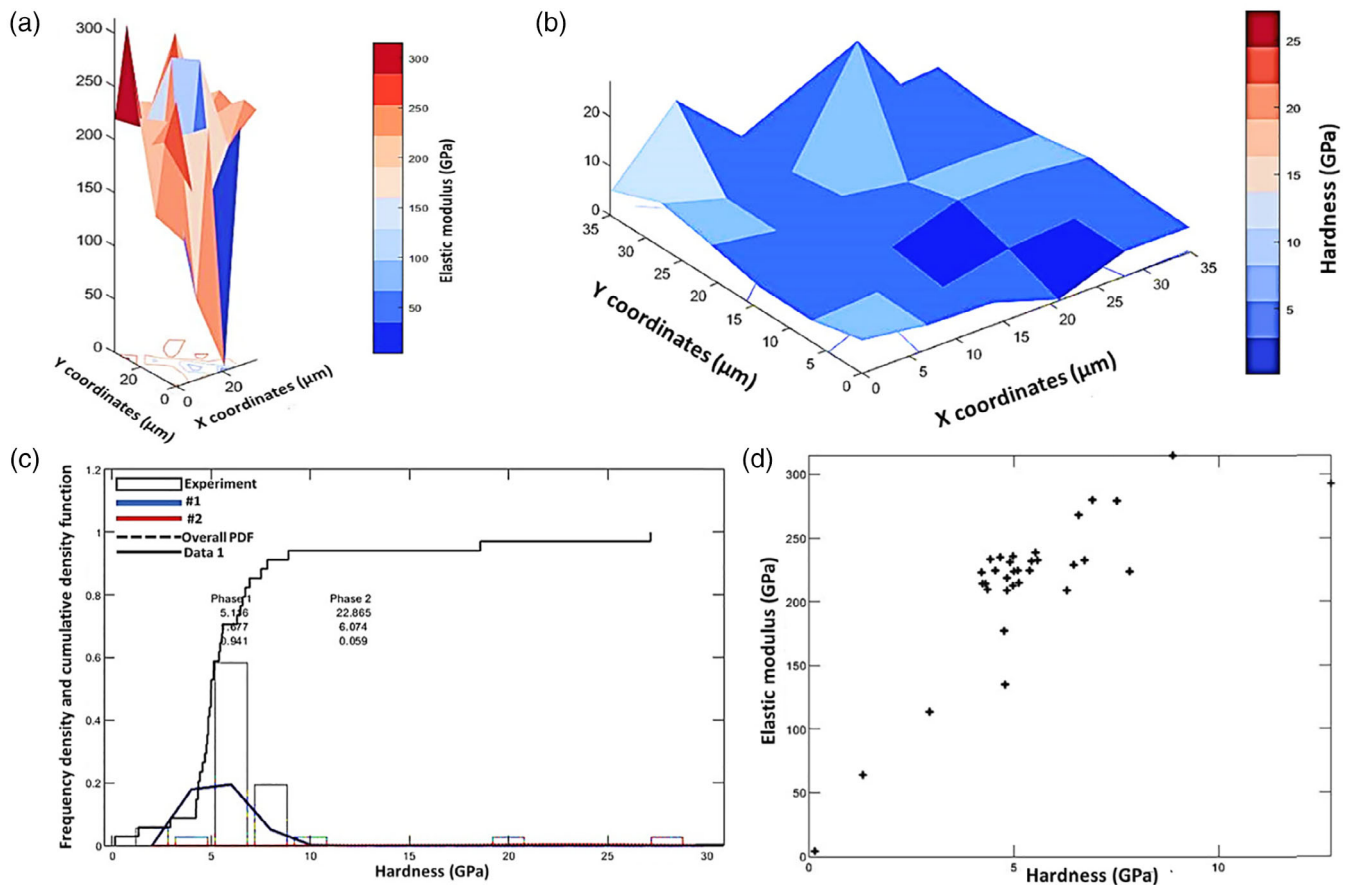


FIGURE 8 (a) Statistical deconvolution mapping of elastic modulus (b) statistical deconvolution mapping of hardness (c) elastic modulus versus hardness (d) probability density function (PDF) and cumulative density function (CDF) versus hardness (GPa) [Color figure can be viewed at wileyonlinelibrary.com]

TABLE 3 Results of the statistical deconvolution mapping of mechanical properties from indentation experiments

Mechanical property	Mean property value (GPa)	Number of points in array	Spacing between indents (μm)
Young's modulus (E)	11.57 ± 46.75	36	7
Hardness (H)	6.01 ± 3.8	36	7

TABLE 4 Estimated values of Hardness (GPa) from PDF and CDF

	Phase 1 of PDF (hardness in GPa)	Phase 2 of PDF (hardness in GPa)
Maximum value	5.116	22.865
Mean value	1.677	6.074
Minimum value	0.941	0.059

Abbreviation: CDF, cumulative density function; GPa, versus hardness; PDF, probability density function.

mechanical properties (Young's moduli, hardness values, and fracture toughness) of the PVA/PVP blends compares favorably with those of emerging promising materials that are being developed for potential applications in SSEs. Although, the focus of this work is on the mechanical properties of PVP/PVA-based solid electrolytes. This work acknowledges that a detailed optimization of the conductivity is needed to develop electrolytes with optimum conductivity as a function of temperature which will be studied in future work.

ACKNOWLEDGMENTS

The authors would like to acknowledge the financial support from the Pan African Materials Institute (AUST/PAMI/2015 5415-NG) under the World Bank African Centres of Excellence Program as well as the National Space Research and Development Agency (NASRDA) Abuja, Nigeria. Appreciation is also extended to the Worcester Polytechnic Institute (WPI) for their support.

CONFLICT OF INTEREST

There is no competing conflict of interest to influence this work.

AUTHOR CONTRIBUTIONS

Kingsley I. Orisekeh: Data curation (lead); formal analysis (lead); methodology (lead); writing – original draft (lead). **Vitalis Anye:** Conceptualization (supporting); formal analysis (supporting). **Oluwaseun K. Oyewole:** Formal analysis (supporting); methodology (supporting); writing – review and editing (supporting). **Ridwan Ahmed:** Formal analysis (supporting); methodology (supporting). **David K. Orisekeh:** Formal analysis (supporting); methodology (supporting). **Omolara V. Oyelade:** Formal analysis (supporting); methodology (supporting). **Sharafadeen A. Adeniji:** Formal analysis (supporting); methodology (supporting). **Sadiq Umar:** Formal analysis (supporting); writing – review and editing (supporting). **Abdulahakeem Bello:** Conceptualization (supporting); data curation (supporting); formal analysis (supporting); writing – review and editing (supporting). **Winston O. Soboyejo:** Conceptualization (lead); funding acquisition (lead); writing – review and editing (lead).

DATA AVAILABILITY STATEMENT

The data that support the findings of this study are available from the corresponding author upon reasonable request.

ORCID

Winston Soboyejo  <https://orcid.org/0000-0002-0209-1079>

REFERENCES

- [1] L. L. Baranowski, C. M. Heveran, V. L. Ferguson, C. R. Stoldt, *ACS Appl. Mater. Interfaces* **2016**, *8*, 29573.
- [2] K. Orisekeh, B. Singh, Y. Olanrewaju, M. Kigozi, G. Ihekwe, S. Umar, V. Anye, A. Bello, S. Parida, W. O. Soboyejo, *J. Energy Storage* **2021**, *33*, 102042.
- [3] J. Rodríguez, E. Navarrete, E. A. Dalchiale, L. Sánchez, J. R. Ramos-barrado, F. Martín, *J. Power Sources* **2013**, *237*, 270.
- [4] A. A. Sallal, S. A. Salman, A. A. Habeeb, *Int. J. Curr. Res.* **2018**, *10*, 74141.
- [5] D. Mondal, M. M. R. Mollick, B. Bhowmick, D. Maity, M. K. Bain, D. Rana, A. Mukhopadhyay, K. Dana, D. Chattopadhyay, *Prog. Nat. Sci. Mater. Int.* **2013**, *23*, 579.
- [6] M. J. Reddy, S. S. Rao, E. Laxminarsaiah, U. V. S. Rao, *Solid State Ionics* **1995**, *80*, 93.
- [7] K. Sundaramahalingam, M. Muthuvinayagam, N. Nallamuthu, D. Vanitha, M. Vahini, *Polym. Bull.* **2019**, *76*, 5577.
- [8] E. M. Abdelrazek, I. S. Elashmawi, A. El-khodary, A. Yassin, *Curr. Appl. Phys.* **2010**, *10*, 607.
- [9] I. Yoon, S. Jurng, D. P. Abraham, B. L. Lucht, P. R. Guduru, *Energy Storage Mater.* **2020**, *25*, 296.
- [10] E. Peled, S. Menkin, *J. Electrochem. Soc.* **2017**, *164*, A1703.
- [11] K. Xu, *Chem. Rev.* **2014**, *114*, 11503.
- [12] W.-J. Zhang, *J. Power Sources* **2011**, *196*, 13.
- [13] K. Xu, *Chem. Rev.* **2004**, *104*, 4303.
- [14] J. Xu, L. Wang, J. Guan, S. Yin, *Mater. Des.* **2016**, *95*, 319.
- [15] G. Yan, J. F. Nonemacher, H. Zheng, M. Finsterbusch, J. Malzbender, M. Krüger, *J. Mater. Sci.* **2019**, *54*, 5671.
- [16] G. Yan, S. Yu, W. Yang, X. Li, H. Tempel, H. Kungl, R. A. Eichel, M. Krüger, J. Malzbender, *J. Power Sources* **2019**, *437*, 226940.
- [17] C. D. Fincher, D. Ojeda, Y. Zhang, G. M. Pharr, M. Pharr, *Acta Mater.* **2020**, *186*, 215.
- [18] G. M. Pharr, W. C. Oliver, *MRS Bull.* **1992**, *17*, 28.
- [19] W. C. Oliver, G. M. Pharr, *J. Mater. Res.* **1992**, *7*, 1564.
- [20] J. Malzbender, G. De With, *Surf. Coat. Technol.* **2001**, *137*, 72.
- [21] J. Malzbender, G. De With, *Surf. Coat. Technol.* **2000**, *127*, 265.
- [22] A. N. Wang, J. F. Nonemacher, G. Yan, M. Finsterbusch, J. Malzbender, M. Krüger, *J. Eur. Ceram. Soc.* **2018**, *38*, 3201.
- [23] J. F. Nonemacher, C. Hüter, H. Zheng, J. Malzbender, M. Krüger, R. Spatschek, M. Finsterbusch, *Solid State Ionics* **2018**, *321*, 126.
- [24] International Organization for Standardization, “ISO 14577-1: 2002, Metallic Materials, Instrumented Indentation Test for Hardness and Materials Parameters-Part 1: Test Method,” <https://www.iso.org/standard/30104.html>.
- [25] S. B. Aziz, M. A. Rasheed, A. M. Hussein, H. M. Ahmed, *Mater. Sci. Semicond. Process.* **2017**, *71*, 197.
- [26] H.-D. Wu, I.-D. Wu, F.-C. Chang, *Polymer* **2001**, *42*, 555.
- [27] S. B. Aziz, R. M. Abdullah, *Electrochim. Acta* **2018**, *285*, 30.
- [28] R. M. Hodge, *Polymer* **1996**, *37*, 1371.
- [29] W. Dong, J. S. Sakamoto, B. Dunn, *Sci. Technol. Adv. Mater.* **2003**, *4*, 3.
- [30] S. Yu, R. D. Schmidt, R. Garcia-Mendez, E. Herbert, N. J. Dudney, J. B. Wolfenstine, J. Sakamoto, D. J. Siegel, *Chem. Mater.* **2016**, *28*, 197.
- [31] L. S. de Vasconcelos, R. Xu, J. Li, K. Zhao, *Extrem. Mech. Lett.* **2016**, *9*, 495.
- [32] Y. Wang, W. H. Zhong, *ChemElectroChem* **2015**, *2*, 22.
- [33] C. Ravindra, M. Sarswati, G. Sukanya, P. Shivalila, Y. Soumya, *Res. J. Phys. Sci.* **2015**, *3*, 1.

How to cite this article: K. Orisekeh, V. Anye, O. Oyewole, R. Ahmed, D. Orisekeh, O. Oyelade, S. Adeniji, S. Umar, A. Bello, W. Soboyejo, *J. Appl. Polym. Sci.* **2022**, e52379. <https://doi.org/10.1002/app.52379>